



Unveiling the Contribution of Lactic Acid to the Passivation Behavior of Ti–6Al–4V Fabricated by Laser Powder Bed Fusion in Hank's Solution

Yu-Hang Chu¹ · Liang-Yu Chen^{1,2} · Bo-Yuan Qin¹ · Wenbin Gao^{1,2} · Fanmin Shang¹ · Hong-Yu Yang³ · Lina Zhang¹ · Peng Qin⁴ · Lai-Chang Zhang⁴

Received: 12 June 2023 / Revised: 22 July 2023 / Accepted: 27 July 2023 / Published online: 19 September 2023
© The Chinese Society for Metals (CSM) and Springer-Verlag GmbH Germany, part of Springer Nature 2023

Abstract

In actual physiological environments, bacteria can activate the immune system and release lactic acid. However, the detailed contribution of lactic acid to the passivation behavior of titanium (Ti) alloys is still unclear. The current work investigated the in vitro passivation behavior of Ti–6Al–4V (TC4) alloys fabricated by laser powder bed fusion in Hank's solution with and without adding lactic acid. Electrochemical methods, inductively coupled plasma atomic emission spectrometer, and X-ray photoelectron spectroscopy were jointly used. Adding lactic acid decreases the corrosion resistance of samples by degrading the formed passive film. The film formed in the (lactic acid)-containing solution exhibits a higher level of oxygen vacancies and a lower thickness, attributed to the suppressed formation of Ti⁴⁺ transformed from Ti³⁺ and Ti²⁺. Moreover, the presence of lactic acid would increase the open circuit potential, relieve the ions release, and hinder the deposition of calcium phosphates within 24 h immersion.

Keywords Titanium alloy · Corrosion behavior · Passive film · Lactic acid · Laser powder bed fusion

1 Introduction

Pure Ti and Ti alloys are widely recognized as suitable materials for implants because of their exceptional mechanical performances, robust corrosion resistance, and good

biocompatibility [1, 2]. Ti implants always come in complex shapes, and their traditional subtractive methods for production involving multiple process steps are time, material, and energy-intensive [3]. Recent decades have witnessed the development of additive manufacturing technologies, including laser powder bed fusion (L-PBF), introduced to produce complex-shaped metallic parts [4–6]. The L-PBF process employs a laser to layer-wisely build up materials in a powder bed based on computer-aided design (CAD) models, facilitating the production of customized surgical implants [7–9]. Compared to conventional techniques, L-PBF technology offers significant advantages, making it an attractive option for producing complex implants.

As the most commonly used material for human implants, Ti alloys are often exposed to physiological environments, generating passive films on their surfaces [10–12]. This passive film is in direct contact with the human physiological environment and acts as a barrier to impede the propagation of corrosion processes along the material surface [11–13]. As a result, considerable research has been devoted to understanding the corrosion behavior of Ti alloys fabricated by L-PBF and the formation of a passive film in physiological environments. Chen et al. [14] compared the corrosion behavior of L-PBF-produced TC4 alloy in dynamic and

Available online at <http://link.springer.com/journal/40195>

✉ Liang-Yu Chen
lychen@just.edu.cn

✉ Hong-Yu Yang
yanghongyu2021@jlu.edu.cn

✉ Lai-Chang Zhang
lczhangimr@gmail.com; l.zhang@ecu.edu.au

¹ School of Materials Science and Engineering, Jiangsu University of Science and Technology, Zhenjiang 212100, China

² Foshan (Southern China) Institute for New Materials, Foshan 528200, China

³ Key Laboratory of Automobile Materials, Ministry of Education and Department of Materials Science and Engineering, Jilin University, Changchun 130025, China

⁴ Centre for Advanced Materials and Manufacturing, School of Engineering, Edith Cowan University, 270 Joondalup Drive, Joondalup, Perth, WA 6027, Australia

static Hank's solutions. They discovered that the flowing solution degrades the corrosion resistance of the alloy and promotes the deposition of calcium phosphates. Cui et al. [15] found that L-PBF-produced TC4 exhibits more severe metastable pitting corrosion than annealed TC4 due to the presence of α' phase in the microstructure. Cabrini et al. [16] heat-treated the L-PBF-produced TC4 alloys and tailored their microstructures, and the heat-treated sample exhibited a higher current density during a short-term potentiostatic polarization in a simulating body fluid.

The actual physiological environments to which implants are exposed are significantly more intricate than the laboratory conditions used for testing. For instance, after implantation, streptococcus mitis can generate lactic acid, which negatively impacts the pH value on the implant surface, ultimately affecting the corrosion behavior of the implant [17]. Furthermore, the oral cavity harbors a polymicrobial ecosystem of Gram- and Gram+ bacteria, which can stimulate the immune system and release lactic acid [18, 19]. Consequently, it is crucial to examine the corrosion behavior of Ti alloys in simulated body fluid (SBF) supplemented with lactic acid. Mabileau et al. [20] reported that lactic acid destabilizes the integrity of passive films, reducing the re-passivation of Ti implants. Benea et al. [21] found that adding lactic acid increases the open circuit potential and polarization resistance of TC4 after 120 h of immersion in Hank's solution. Alexandra et al. [22] compared the corrosion resistance of L-PBF-produced and wrought TC4 in 0.1 M lactic acid + 0.1 M NaCl solution after 1150 h of immersion at 37 °C and found that L-PBF-produced TC4 shows good corrosion resistance as compared to wrought TC4 in such an environment. Qu et al. [23] discovered that increasing the amount of lactic acid in artificial saliva causes the corrosion rate of Ti to rise, decreasing the impedance of the passive film. Although it is generally found that the lactic acid could decrease the corrosion resistance of Ti alloys, many scientific questions, such as the passivation behavior, semiconductive properties, formation and dissolution of passive films in the SBF with different lactic acid contents, remain unanswered, particularly concerning additively manufactured Ti alloys. Therefore, to leverage the potential of L-PBF-produced Ti alloys in biomedical applications, it is necessary to investigate the influence of lactic acid on the passivation performance of L-PBF-produced TC4 in SBF.

As such, L-PBF-produced TC4 alloy was selected as the focal point of this work, and Hank's solutions with varying contents of lactic acid were used as electrolytes. Multiple methods were employed to explore the passivation characteristics of TC4 alloy produced by L-PBF and the creation and breakdown of passive films in Hank's solution with the addition of lactic acid. Furthermore, the work included a discussion of the mechanisms underlying the influence of lactic acid on the corrosion of L-PBF-produced TC4 alloy.

2 Experimental

2.1 Materials and Solution

TC4 cubes measuring 10 mm × 10 mm × 10 mm were fabricated via an MTT SLM250 HL machine. The metallic powder was produced via gas atomization of a TC4 ingot and presented a distribution of $D_{50} = 39.5 \mu\text{m}$. The manufacture of TC4 via L-PBF was carried out in a high-purity argon environment. The parameters employed included: a laser power of 200 W, a spot size of 80 μm , a laser scan speed of 1000 mm/s, a layer thickness of 50 μm , and a hatch spacing of 100 μm . Each successive layer has a 90-degree rotation in the scanning direction. The Archimedes method revealed a relative density > 99.5% for the produced TC4 cubes. All samples examined in this research remained in their original processed state and underwent no post-processing procedures. The specimens utilized for electrochemical evaluations were strung with copper wires and sealed with epoxy resin. The surface underwent sanding using waterproof SiC sandpaper up to 2000 grit, followed by a mirror finish polishing using a diamond polishing paste. Additionally, silicone (Kafuter 704RTV) was used to seal the sample edges between metal and resin to prevent crevice corrosion. In this study, the electrolyte used was Hank's solution, prepared by adding 0.35 g/L NaHCO_3 to Hank's balanced salt solution (produced by Heart Biological Technology Co. LTD., China). Hank's salt primarily consists of 0.140 g/L CaCl_2 , 0.4 g/L KCl, 0.06 g/L KH_2PO_4 , 0.098 g/L MgSO_4 , 8 g/L NaCl, 1 g/L $\text{C}_6\text{H}_{12}\text{O}_6$, 0.048 g/L Na_2HPO_4 and 0.011 g/L $\text{C}_{19}\text{H}_{14}\text{O}_5\text{SNa}$. Accordingly, lactic acid was added to achieve pH values of 7, 5 and 3 for Hank's solution. Samples immersed in solutions with pH = 7, pH = 5 and pH = 3 were denoted as Ti7, Ti5, and Ti3 to facilitate the following description. The solution temperature was constant at $37 \pm 0.5 \text{ }^\circ\text{C}$ during the electrochemical measurements and immersion tests. All reagents employed in this investigation were of analytical grade, and distilled water was used to prepare Hank's solution.

2.2 Microstructural Characterizations

Samples for microstructural analysis were subjected to standard metallographic procedures and then immersed in Kroll's reagent ($\text{H}_2\text{O} : \text{HNO}_3 : \text{HF} = 85 : 10 : 5$, in vol.%) for etching purposes. Optical microscopy (OM) and scanning electron microscopy (SEM), respectively, utilizing Axioskop2-MAT (Zeiss) and Sigma HD (Zeiss) equipped with an energy dispersive X-ray spectrometer (EDS) detector, were employed to observe the microstructures of the

alloy samples after etching or corrosion. For transmission electron microscopy (TEM, JEM-2100F, JEOL) observation, the samples were initially ground to approximately 100 μm in size. Subsequently, the final thinning process was carried out utilizing a twin-jet polishing machine at a temperature of $-30\text{ }^\circ\text{C}$, using a mixture solution containing HClO_4 : $\text{C}_4\text{H}_9\text{OH}$: CH_3OH in a volumetric ratio of 1:3:6. For phase constituent analysis of L-PBF-produced TC4, an X-ray diffractometer (Empyrean, PANalytical) equipped with $\text{Co-K}\alpha$ radiation was employed. The X-ray diffraction (XRD) scanning range was configured from 35° to 100° , with a scanning rate of $0.03^\circ/\text{s}$. Jade 6.5 software was used to analyze the XRD data.

2.3 Electrochemical Measurements

The electrochemical behavior of the samples was examined using a CHI660E electrochemical workstation equipped with a three-electrode system (Chenhua). The working electrode was the L-PBF-produced TC4 sample, while a Pt sheet was employed as the counter electrode, and a saturated calomel electrode (SCE) was utilized as the reference electrode. All reported potentials were referenced to SCE. The open circuit potential (OCP) of the samples was tested for 1800s to ensure the stability of the samples in the solution. Afterward, electrochemical impedance spectroscopy (EIS) was conducted through a potentiostatic methodology, where a sinusoidal voltage signal with a peak-to-peak amplitude of 10 mV was applied. The frequency range for the measurement spanned from 10^5 to 10^{-2} Hz. The acquired data from EIS were analyzed and fitted utilizing the ZsimpWin software.

Subsequently, potentiodynamic polarization tests were carried out by scanning the potential from -0.25 to $+2$ V (vs. OCP) at a scan rate of 0.1667 mV/s. The resulting potentiodynamic polarization data were analyzed and fitted using Cview software. During the potentiostatic polarization, passive films were generated on the surfaces of the L-PBF-produced TC4 samples. According to the passivation area obtained from the polarization curve, 0.6 V, 0.7 V, 0.8 V, 0.9 V and 1.0 V were chosen for a 0.5 h potentiostatic polarization. At each potentiostatic potential, EIS measurements were carried out, and the ensuing data were processed employing the ZsimpWin software. The effective capacitance, measured at a frequency of 1 kHz, was utilized to calculate the film thickness. In addition, Mott–Schottky tests were carried out at 1 kHz. The potential was swept from the film formation potential to -1 V using a rate of 10 mV/s. Each electrochemical test has been repeated a minimum of three times to ensure the reproducibility of data.

2.4 Ion Concentration Test

Potentiostatic polarization tests were conducted for three distinct groups of samples in varying pH solutions. Subsequently, the samples and solutions were immersed in a beaker for 24 h. The beaker was sealed with plastic film to prevent electrolyte evaporation during immersion. Following the 24 h immersion, the electrolyte was analyzed for Ti, Al and V ion concentrations using an inductively coupled plasma atomic emission spectrometer (ICP-AES, 7700x, Agilent).

2.5 Compositions of Passive Films

Extensive analysis was performed on the compositions of the passive films on the samples after potentiostatic polarization under the potential of 0.6 V using X-ray photoelectron spectroscopy (XPS, Thermofischer, ESCALAB 250XI). An Al K_α X-ray source with the photon energy ($h\nu$) of 1486.6 eV was utilized. The voltage and current were 15 kV and 10 mA. The spot diameter was approximately 500 μm , and the test durations varied between 0 s, 10 s, 30 s and 60 s. Ar ion etching, which exhibits an etch rate of roughly 0.2 nm/s, was utilized on the sample surface. The $\text{C}1s$ standard peak (with a binding energy of 284.6 eV) was utilized to calibrate the XPS spectra. The fitting of the XPS results was performed using Avantage software.

3 Results

3.1 Microstructure Analysis

Figure 1 shows the microstructure features of L-PBF-produced TC4. Figure 1a portrays the XRD pattern of L-PBF-produced TC4. As a dual-phase alloy, the L-PBF-produced TC4 shows no detected β -phase peak, resulting from the limited diffusion of V during the fabrication. Similar findings are also reported primarily because the diffusion of β -stabilizing V in the melt is restricted during the L-PBF process due to rapid cooling [24–27]. Under OM observation, the microstructure of as-fabricated TC4 demonstrates a considerable presence of the needle-like α' martensitic phase (Fig. 1a). This needle-like martensitic phase, which is produced due to rapid cooling from the β region to the α region, is frequently observed in Ti alloys and other hexagonal close-packed (HCP) metals, as reported in previous literature [28, 29]. Figure 1c and d represent the bright-field and dark-field TEM images for the microstructure of the sample. A significant quantity of needle-shaped α' martensite is also observed. The rapid cooling rate of the material inevitably leads to the generation of high residual stresses, consequently giving rise to lattice defects. The presence of

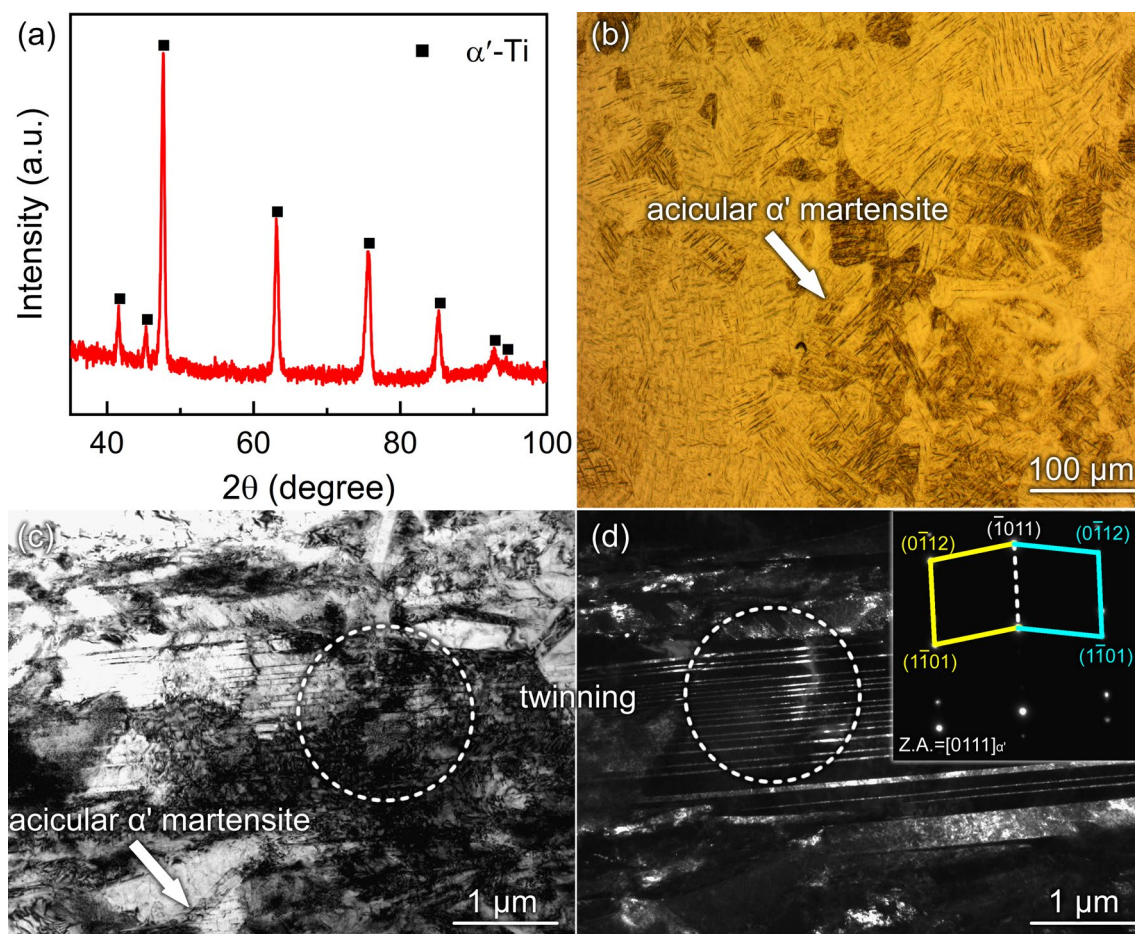


Fig. 1 Microstructural features of L-PBF-produced TC4 sample: **a** XRD pattern, **b** optical microstructure, **c** bright-field TEM image, **d** dark-field TEM image (inset is the selected area diffraction pattern in the dashed circle)

dislocations in the TEM bright-field image frequently manifests as a darker contrast owing to electron beam interference, providing visual evidence of lattice distortion. The inset in Fig. 1d indicates the twinning grains have the HCP structure.

3.2 Electrochemical Tests

Figure 2 represents the OCP curves of as-fabricated samples in Hank's solution with different pH values at 37 °C. The OCPs of the samples show variability, which can be attributed to the formation of distinct oxide films on the surfaces of the samples, as illustrated in Fig. 2. In the case of TC4 in Hank's solution with pH=5 and pH=3, the OCPs from the onset to the equilibrium state are found to be consistently higher than that without lactic acid addition. This higher OCP is attributable to the absorption of lactic acid on the sample surfaces during immersion, which impedes the contact of the sample surface with the solution [21].

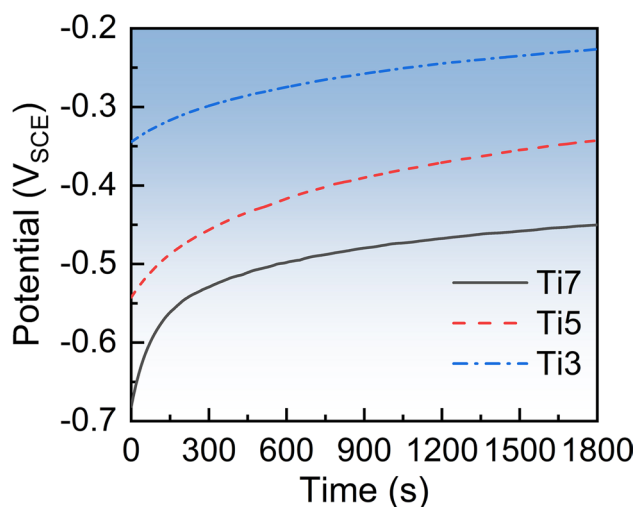


Fig. 2 OCP curves of L-PBF-produced TC4 in Hank's solutions at 37 °C with different pH values controlled by lactic acid. Ti7, Ti5, and Ti3 indicate the samples in Hank's solutions with pH values of 7, 5 and 3

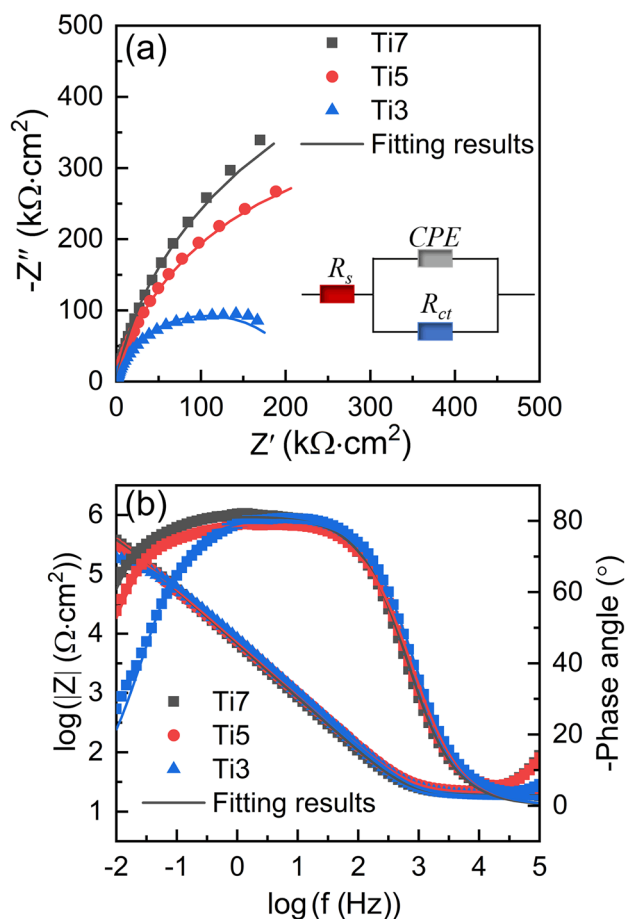


Fig. 3 Electrochemical impedance spectroscopies of L-PBF-produced TC4 samples in Hank's solutions with different lactic acid concentrations at 37 °C: **a** Nyquist plots, **b** Bode plots. Inset in **a** is the equivalent electrical circuit fitting the EIS results. Ti7, Ti5, and Ti3 indicate the samples in Hank's solutions with pH values of 7, 5, and 3

The Nyquist and Bode plots of samples are illustrated in Fig. 3a and b. As evident in Fig. 3b, the capacitive loop of Ti7 displays a larger radius than those of Ti5 and Ti3. In the Nyquist diagram, the loop radius indicates the impedance of the passive film on the sample; a larger capacitive loop radius corresponds to a higher impedance of the passive film [14]. According to this phenomenon, the impedance of the passive film formed on Ti7 after the OCP test is higher than those of Ti5 and Ti3. The Bode impedance plots shown in Fig. 3b exhibit two distinct regions. The curve indicates the electrolyte resistance, remaining flat within the mid-high frequency range of 10^3 – 10^5 Hz. The impedance exhibits a linear increase in the frequency region of 10^{-2} to 10^3 Hz as the frequency decreases. The Bode phase angle diagram also indicates that the resistance of the electrolyte remains constant in EIS measurement, with a phase angle close to 0° at high frequencies [30]. The curves in the mid-frequency region have a platform shape and are near 80° , specifying

Table 1 Fitting results of electrochemical impedance spectroscopies for L-PBF-produced TC4 in Hank's solutions with and without lactic acid

Sample	R_s (Ω cm 2)	$CPE \times 10^{-6}$ (Ω^{-1} s n cm $^{-2}$)	n	R_{ct} ($M\Omega$ cm 2)
Ti7	21.07 ± 1.83	29.38 ± 1.93	0.90 ± 0.02	1.07 ± 0.24
Ti5	20.94 ± 1.75	27.56 ± 2.87	0.88 ± 0.02	0.75 ± 0.15
Ti3	18.18 ± 1.89	23.98 ± 2.32	0.90 ± 0.01	0.22 ± 0.14

that the passive films on the samples are compact [5, 31]. In the low-frequency region, the phase angle demonstrates a decreasing trend: Ti7 > Ti5 > Ti3. The difference indicates that the content of lactic acid significantly influences the formed passive film in Hank's solution. To determine the capacitance of the passivation films formed on the sample surfaces, an equivalent electrical circuit model $R(QR)$ is employed to fit the EIS data. In this equivalent electrical circuit model, R_s represents the solution resistance, CPE is the constant phase element, and R_{ct} symbolizes the charge transfer resistance. Due to the complex corrosive environment, the passive film capacitor does not exhibit ideal behavior, and CPE is utilized to introduce frequency dispersion, with the value determined by the following equation [32, 33]:

$$Z_{CPE} = \frac{1}{Q(j\omega)^n}, \quad (1)$$

where ω denotes the angular frequency (in radians per second), j represents the imaginary unit ($j^2 = -1$), and Q indicates the constant specific to the constant phase element (CPE). The exponent n corresponds to a parameter, and when given the value of 1, the CPE functions ideally as a capacitor. When n varies within the range from 0.5 to 1, the CPE operates as a non-ideal capacitor, whereas when n equals 0, the CPE is understood to act as a resistance [34]. The outcomes of the fitting procedure for the EIS curves in Fig. 2 are presented in Table 1. The parameter R_{ct} represents the resistance associated with the charge transfer process from the metal to the solution. The order of resistances of the samples is as follows: Ti7 (1.07 ± 0.24 $M\Omega$ cm 2) > Ti5 (0.75 ± 0.15 $M\Omega$ cm 2) > Ti3 (0.22 ± 0.14 $M\Omega$ cm 2). As a result, the introduction of lactic acid in Hank's solution gradually decreases the protectiveness of passive film on the surfaces of L-PBF-produced TC4.

Figure 4 represents the potentiodynamic polarization plots of the Ti7, Ti5, and Ti3 samples. The potentiodynamic polarization curves of all samples display a consistent pattern of typical passivation behavior. The authors have also performed a fitting analysis of the potentiodynamic polarization curves, and the results are reported in Table 2. The corrosion potential values have been estimated and demonstrate the following order among the samples:

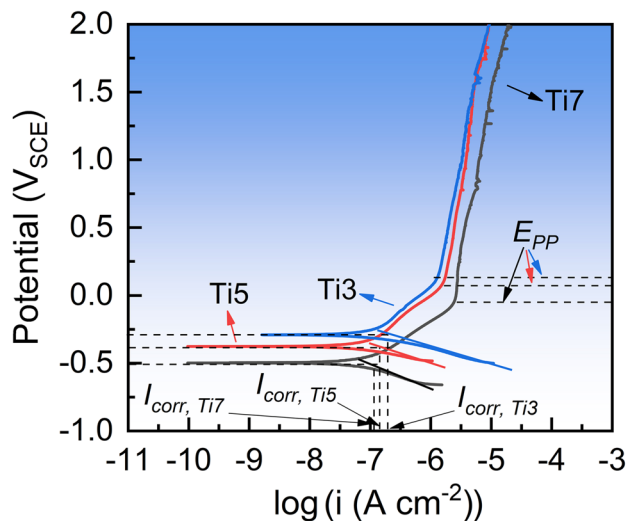


Fig. 4 Potentiodynamic polarization curves of L-PBF-produced TC4 samples in Hank's solutions with different lactic acid concentrations at 37 °C. Ti7, Ti5, and Ti3 indicate the samples in Hank's solutions with pH values of 7, 5 and 3

Table 2 Fitted potentiodynamic polarization results of Ti7, Ti5 and Ti3 samples in Hank's solution at 37 °C

Sample	I_{corr} ($\mu\text{A cm}^{-2}$)	E_{corr} (V)	E_{pp} (V)	Corrosion rate $\times 10^{-5}$ (mm y^{-1})
Ti7	0.12 ± 0.02	-0.49 ± 0.06	-0.043 ± 0.05	0.33 ± 0.11
Ti5	0.15 ± 0.03	-0.37 ± 0.06	0.081 ± 0.07	0.43 ± 0.14
Ti3	0.18 ± 0.03	-0.29 ± 0.08	0.139 ± 0.06	0.49 ± 0.16

I_{corr} is the corrosion current density, and E_{corr} is the corrosion potential

Ti7 samples (-0.49 ± 0.06 V) < Ti5 (-0.37 ± 0.06 V) < Ti3 (-0.29 ± 0.08 V). This observation upholds the prior OCP results assessment. Moreover, it has been noted that E_{corr} , which represents the energy associated with the corrosion reaction, suggests that the Ti7 sample necessitates lower oxidation energy than the Ti5 and Ti3 samples. Correspondingly, the passivation potential values also have the following order among the samples: Ti7 samples (-0.043 ± 0.05 V) < Ti5 (0.081 ± 0.07 V) < Ti3 (0.139 ± 0.06 V). Additionally, the fitting analysis has yielded values for the corrosion current densities that pertain to Ti7, Ti5 and Ti3 samples, which equal $0.12 \pm 0.02 \mu\text{A cm}^{-2}$, $0.15 \pm 0.03 \mu\text{A cm}^{-2}$ and $0.18 \pm 0.03 \mu\text{A cm}^{-2}$, respectively [35]:

$$\text{Corrosion rate} = \frac{MI_{\text{corr}}}{nF\rho_m}, \quad (2)$$

in the equation, M represents the molar mass of Ti (47.87 g/mol), n denotes the charge of the Ti ion, F represents the

Faraday constant ($96,487 \text{ C mol}^{-1}$), and ρ_m is the density (4.43 g/cm^3 for TC4). Upon calculation, the corrosion rates of Ti7, Ti5, and Ti3 are $0.33 \pm 0.11 \times 10^{-5} \text{ mm/y}$, $0.43 \pm 0.13 \times 10^{-5} \text{ mm/y}$ and $0.49 \pm 0.16 \times 10^{-5} \text{ mm/y}$, respectively. This finding indicates that the samples are more prone to corrosion in acidic solutions. Moreover, as the content of lactic acid augments, the corrosion resistance of the sample gradually decreases. It should be noted that for acidic solutions, especially those with added lactic acid, the cathodic region of the potentiodynamic polarization curve exhibits a larger current density attributed to hydrogen reduction and evolution processes taking place in that region [36].

3.3 Potentiostatic Polarization and Its Electrochemical Impedance Spectroscopy

A series of film-forming potentials ranging from 0.6 to 1.0 V are selected according to the passivation region in the potentiodynamic polarization curves to produce oxide films (Fig. 4). Figure 5 is the potentiostatic polarization curves and corresponding double logarithmic curves from 0.6 to 1 V. All potentiostatic polarization curves show the same pattern with a rapid decline in current density over time, indicating the formation of a passive film on the sample. The insets within Fig. 5a, c, and e magnify the curves between 1500 and 1800 s. During this interval, the quasi-steady-state current density (i_{ss}) declines notably, whereby applying a high potential generates a higher current density relative to a low potential application [37]. The growth kinetics of the passive film, as proposed by Macdonald's model, can be fitted with the following equation [38]:

$$\log i_{\text{ss}} = \log A + n \log t, \quad (3)$$

in the equation, A and n are constants, and t is the polarization time. When n is close to -1 , the formed passive film is denser and has higher protection [30]. The fitting results of n for Ti7 are generally larger than those for Ti5 and Ti3. After potentiostatic polarization under 1 V, the values of n for Ti7, Ti5 and Ti3 are -0.77 ± 0.02 , -0.68 ± 0.03 and -0.64 ± 0.02 , respectively, indicating that the passive film on Ti7 is denser compared to those on Ti5 and Ti3.

Figure 6 illustrates the EIS results of Ti7, Ti5 and Ti3 samples after undergoing potentiostatic polarization at various applied potentials ranging from 0.6 to 1.0 V. A larger capacitive loop radius on the Nyquist plot indicates an increased difficulty in the charge transfer between the sample and the solution. This finding implies an increased impedance of the passive films in response to the applied potential increase [39]. As demonstrated in the EIS curve, the passive film manifests a double-layer structure (consisting of a porous outer layer and a dense inner layer)

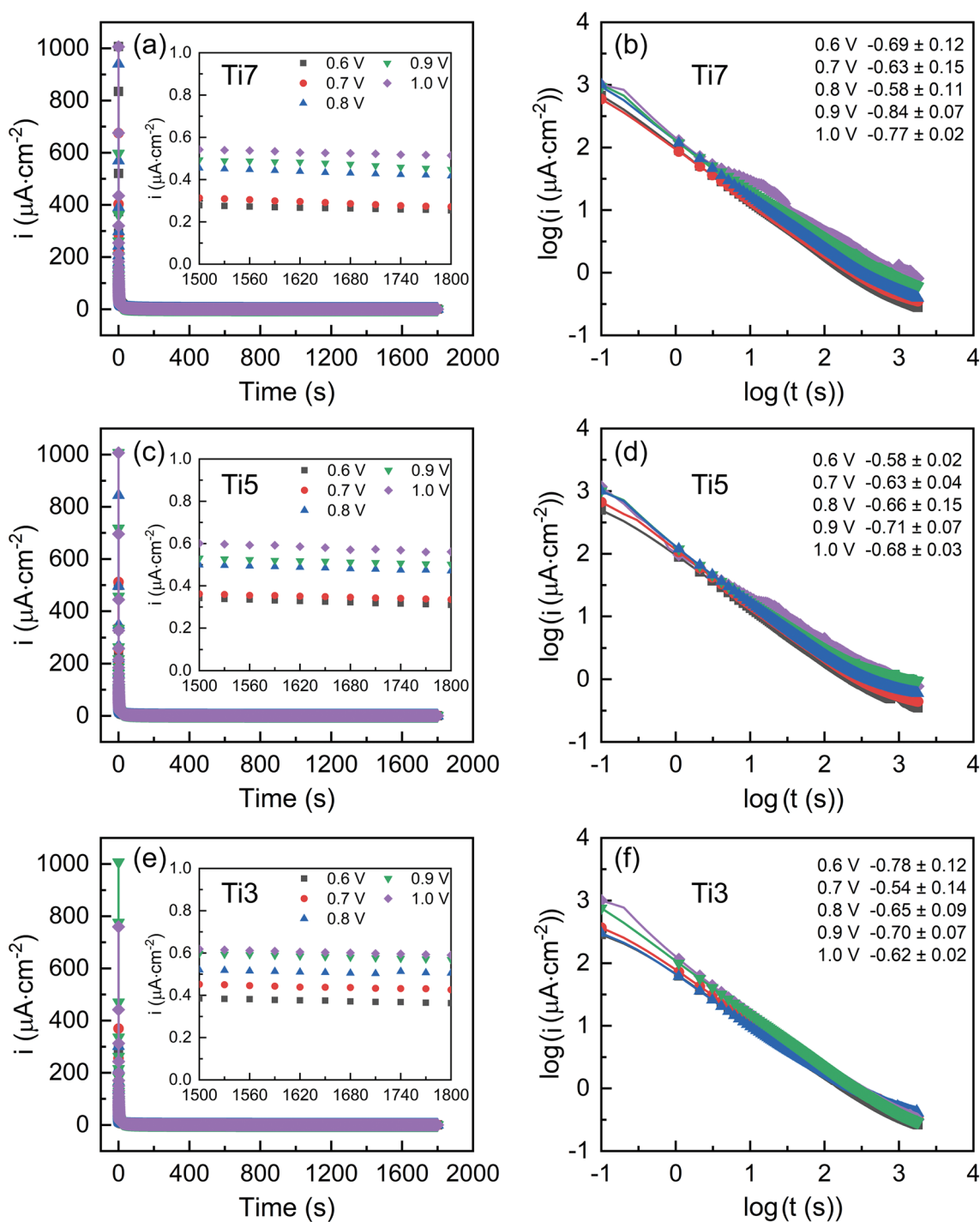


Fig. 5 Potentiostatic polarization curves and corresponding double logarithmic curves from 0.6 to 1 V: **a, b** Ti7, **c, d** Ti5 and **e, f** Ti3. Insets are enlarged images from 1500 to 1800 s. Ti7, Ti5 and Ti3 indicate the samples in Hank's solutions with pH values of 7, 5 and 3

[40, 41]. By utilizing the $R(Q(R(QR)))$ model, an equivalent electrical circuit was employed to fit the EIS results. R_f represents the resistance of the porous outer layer, R_{ct} represents the resistance of the dense inner layer, and CPE denotes the constant phase element. Additionally, CPE_1 and CPE_2 were adopted to illustrate the capacitive

behavior of the dense inner and porous outer layers. The fitting outcome of EIS is presented in Table 3. The R_f value appears to be significantly lower than R_{ct} values for all samples, indicating that R_{ct} mainly determines the corrosion resistance of the samples. Furthermore, Ti7

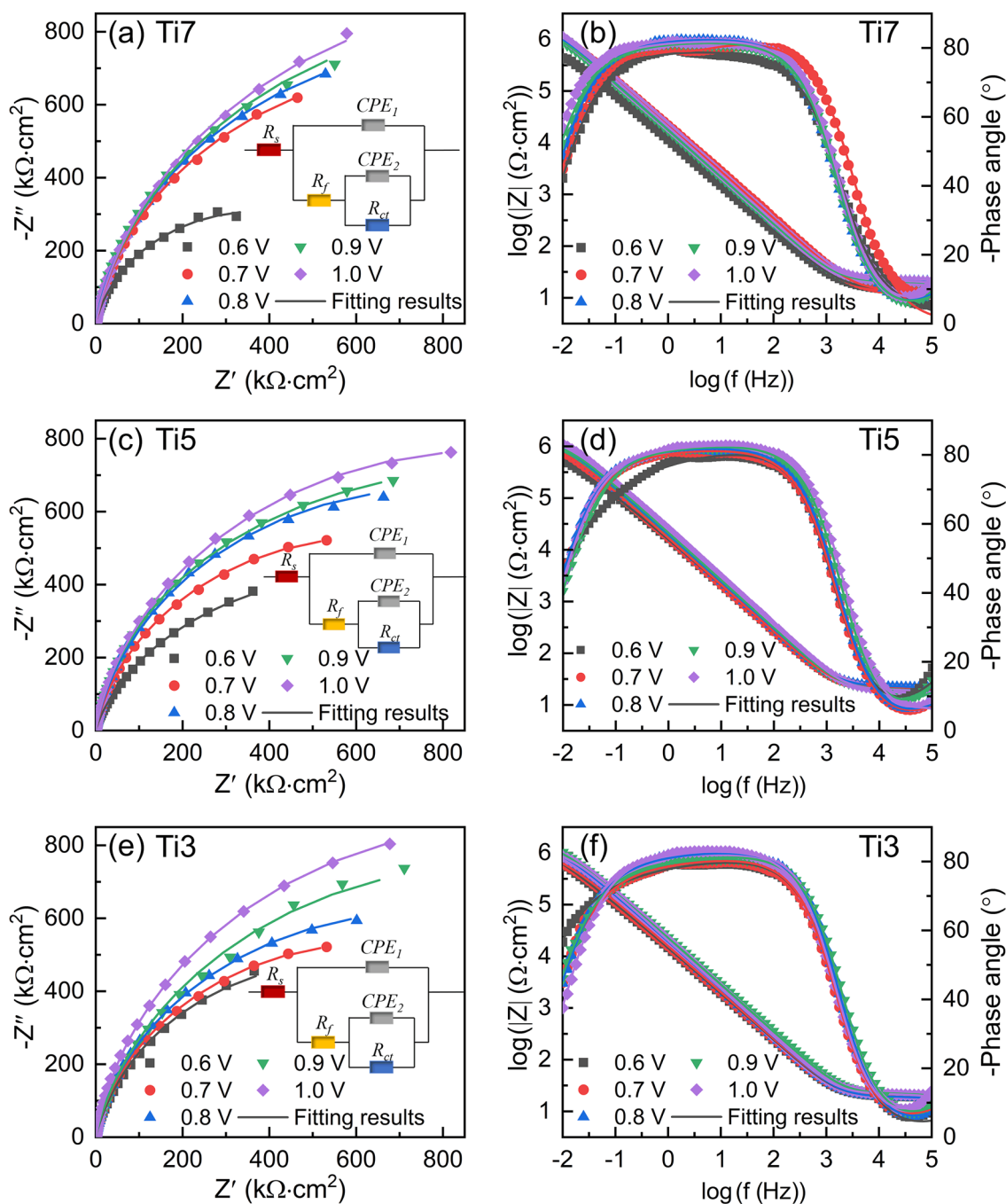


Fig. 6 Electrochemical impedance spectroscopy for the L-PBF-produced TC4 after potentiostatic polarization with different pH values at 37 °C: **a, c and e** Nyquist diagram, **b, d and f** Bode diagram. Ti7, Ti5 and Ti3 indicate the samples in Hank's solutions with pH values of 7, 5 and 3

demonstrated the highest R_{ct} value among all samples in compliance with the applied potential increment, following the Ti7 > Ti5 > Ti3 pattern. Consequently, the presence of lactic acid in the Hank's solution decreased the corrosion resistance of L-PBF-produced TC4 potentiostatic polarized at 37 °C.

3.4 Semiconductive Properties of Passive Films

The production of passive films on metal surfaces during the corrosion process can be ascribed to the movements of ions and point defects, as reported in Ref. [38]. In this regard, $M-S$ tests were performed after potentiostatic polarization under various applied potentials. Figure 7 illustrates that the positive slopes of $M-S$ curves in the range of -0.5

Table 3 Summarized fitting EDS results from Fig. 6

Sample	Potential (V)	R_s ($\Omega \text{ cm}^2$)	$\text{CPE}_1 \times 10^{-6}$ ($\Omega^{-1} \text{ s}^n \text{ cm}^{-2}$)	n_1	R_f ($\text{k}\Omega \text{ cm}^2$)	$\text{CPE}_2 \times 10^{-5}$ ($\Omega^{-1} \text{ s}^n \text{ cm}^{-2}$)	n_2	R_{ct} ($\text{M}\Omega \text{ cm}^2$)
Ti7	0.6	20.15 ± 0.84	10.95 ± 0.53	0.90 ± 0.03	10.21 ± 0.62	1.05 ± 0.49	0.76 ± 0.12	1.16 ± 0.12
	0.7	21.02 ± 1.05	4.44 ± 0.71	0.96 ± 0.02	12.39 ± 0.57	5.12 ± 0.53	0.86 ± 0.09	1.92 ± 0.28
	0.8	19.02 ± 1.59	8.62 ± 0.05	0.86 ± 0.08	13.66 ± 0.74	1.56 ± 0.82	0.97 ± 0.01	2.23 ± 0.35
	0.9	23.34 ± 0.83	2.52 ± 0.26	0.72 ± 0.13	20.57 ± 0.35	5.05 ± 0.07	0.96 ± 0.01	2.46 ± 0.76
	1.0	22.81 ± 2.84	1.19 ± 0.08	0.73 ± 0.07	25.23 ± 0.28	6.37 ± 0.79	0.94 ± 0.02	2.81 ± 0.69
Ti5	0.6	16.38 ± 0.24	1.13 ± 0.45	0.91 ± 0.04	5.48 ± 0.43	2.85 ± 0.63	0.93 ± 0.03	1.06 ± 0.35
	0.7	13.21 ± 1.52	2.51 ± 0.37	0.73 ± 0.15	8.68 ± 0.62	8.75 ± 0.49	0.92 ± 0.04	1.41 ± 0.29
	0.8	14.55 ± 1.03	1.83 ± 0.79	0.76 ± 0.12	9.20 ± 0.84	7.82 ± 0.73	0.93 ± 0.03	1.75 ± 0.17
	0.9	13.49 ± 2.26	2.26 ± 0.93	0.77 ± 0.07	11.72 ± 0.38	6.67 ± 0.39	0.94 ± 0.02	2.38 ± 0.44
	1.0	15.84 ± 0.63	3.55 ± 1.04	0.83 ± 0.11	15.24 ± 0.21	4.16 ± 0.27	0.96 ± 0.01	2.73 ± 0.55
Ti3	0.6	14.76 ± 0.14	4.01 ± 1.43	0.64 ± 0.07	9.32 ± 0.46	5.14 ± 0.23	0.92 ± 0.02	0.91 ± 0.20
	0.7	12.29 ± 0.46	3.57 ± 0.74	0.70 ± 0.06	10.21 ± 0.73	9.31 ± 0.53	0.93 ± 0.05	1.15 ± 0.32
	0.8	10.68 ± 0.96	1.98 ± 0.69	0.73 ± 0.04	12.36 ± 0.26	8.08 ± 0.39	0.94 ± 0.03	1.59 ± 0.27
	0.9	11.84 ± 1.65	2.10 ± 1.26	0.73 ± 0.02	13.51 ± 0.07	6.29 ± 0.58	0.94 ± 0.01	1.81 ± 0.17
	1.0	15.4 ± 2.53	8.89 ± 0.37	0.92 ± 0.14	16.32 ± 0.49	4.87 ± 0.74	0.89 ± 0.08	2.42 ± 0.52

to -0.25 V indicate the presence of typical n -type semiconductive characteristics in the formed passive films. An n -type semiconductive passive film generally comprises oxygen vacancies and/or cation gaps (donors) [42, 43]. Analyzing the semiconductive properties of the passive films more comprehensively can be achieved by calculating the donor density (N_D) based on the slopes of the $M-S$ curves. The slope is equal to $\frac{2}{\epsilon\epsilon_0eN_D}$ according to the $M-S$ expression of n -type semiconductor [44], where ϵ denotes the dielectric constant of the passive film (TiO_2 is equal to 60 [37]), ϵ_0 denotes the vacuum permittivity (8.85×10^{-14} F cm^{-1}), e denotes the electronic charge (1.6×10^{-19} C).

Upon plotting the N_D values of all samples at varying pH values (as illustrated in Fig. 8a), a conspicuous decrease in N_D values of the samples with an increase in the applied potential is observed. Furthermore, it is observed that the passive film exhibits higher N_D values in solutions characterized by lower pH values. Incorporating lactic acid is perceived as highly likely to increase N_D values. The calculation thicknesses (L_{ss}) of passive films after potentiostatic polarization are accomplished using the following equation: [45]:

$$L_{ss} = \frac{\epsilon\epsilon_0A}{C_{\text{eff}}}, \quad (4)$$

where A represents the effective passivation area of the electrode, and C_{eff} represents the effective capacitance obtained from the electrochemical impedance spectroscopy (EIS) data at a frequency of 1000 Hz. Hence, the calculation of passive film thicknesses formed on Ti7, Ti5 and Ti3 sampled surfaces has been executed via Eq. (4), with the obtained results presented in a summarized manner in Fig. 8b. The

L_{ss} results reveal the ordering of the passive film thicknesses created under the same potential whereby $\text{Ti7} > \text{Ti5} > \text{Ti3}$. Further analysis indicates that as the concentration of lactic acid increases, the L_{ss} values decline reciprocally, indicating that higher lactic acid concentrations are non-ideal to produce passive films on L-PBF-produced TC4 surfaces while immersed in Hank's solution.

3.5 Ions Release and Corroded Morphologies

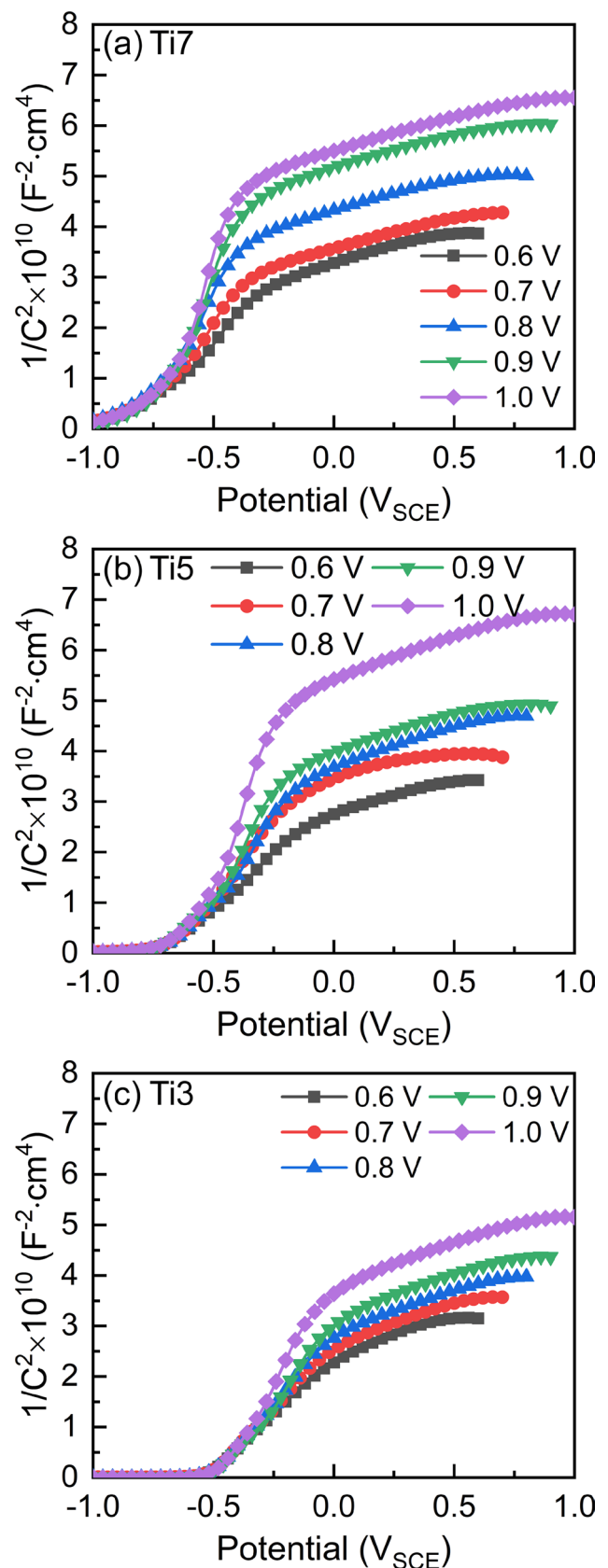
Ti alloys serve as indispensable biomedical materials after being implanted into the human body, where ion release becomes a critical factor that necessitates careful consideration [46]. In a bid to comprehend the ion release of the samples, the concentrations of released Ti, Al and V ions of potentiostatic polarized samples at 0.6 V and after immersion for 24 h were established via ICP-AES analysis, as displayed in Fig. 9a. The examination reveals that the concentrations of released Ti and V ions are relatively identical for all samples. Nonetheless, the Ti3 sample releases a slightly high level of Al ions compared to the Ti5 and Ti7 samples. It is noteworthy that the human body may be susceptible to certain diseases, such as Alzheimer's disease and osteoporosis, upon excessive intake of Al ions [47]. The recommended daily consumption of Al ions by humans should be at most 1 mg/kg [47]. For instance, adults weighing 70 kg should consume less than 70 mg of aluminum (Al) ions daily. This amount encompasses Al ion intake through food and the amount released by the implant. The ion release rates maintained in this work were below the upper limit of human consumption, even when using Ti implants with a surface area that spans several hundred square centimeters and in Hank's

Fig. 7 Mott–Schottky curves of passive films on samples under different concentrations of lactic acid: **a** Ti7, **b** Ti5, **c** Ti3. Ti7, Ti5 and Ti3 indicate the samples in Hank's solutions with pH values of 7, 5, 3

solution even at pH value 3 with only a 1 cm^2 exposed surface of the implanted samples. Prior research studies have reported that Al ions are prone to be released from passive films of Ti alloys [14, 48]. The maximum valence state of Al ion (+3) is lower than that of Ti ion (+4). Hence, an Al ion can pin an oxygen vacancy in the passive film to maintain local electroneutrality [49]. This metastable state of the Al ion and oxygen vacancy pair is easily broken during the passive film dissolution. In addition, in the case of Hank's solution, the high concentration of hydrogen ions presented at a pH of 3 also promotes passive film dissolution [50]. Consequently, a higher concentration of released Al ions is evident in the Ti3 sample.

It has been remarked that various salts, such as $\text{Ca}_3(\text{PO}_4)_2$, hydroxyapatite, and miscellaneous calcium phosphates, tend to deposit on the surface of implanted samples during immersion tests [14, 48]. As the deposits occur discontinuously, obtaining a statistical result of their amounts proves rather tricky. An alternative method was employed to overcome this obstacle, whereby the amount of deposited salt was examined by analyzing residual Ca and P concentrations in Hank's solution after the immersion test. The detected Ca and P concentrations were quantified to establish the amount of deposited salt. As demonstrated in Fig. 9b, the most considerable amount of Ca and P remained in Hank's solution with a pH value of 3, indicating that lactic acid can inhibit calcium phosphate formation. In comparison, the concentration of Ca and P in Hank's solution with a pH value of 7 exceeded those of the other two samples. It has been established that the formation of calcium phosphates on implants can promote osseointegration following implantation [51]. Consequently, the presence of lactic acid serves as an impediment to osseointegration.

Figure 10 shows the morphologies of potentiostatic polarized samples under 0.6 V and 24 h immersion tests. Ti7 shows a flat surface with a few pits (Fig. 10a). Such a finding is also frequently reported by other works in which Ti and Ti alloys are corroded in a neutral solution [14]. In comparison, an appreciable quantity of shallow pits is observed on the Ti5 surface. It is speculated that the pits are produced by the action of lactic acid owing to the etching of H^+ . Nevertheless, the dissolution of passive film is observed besides the shallow pits. It should be pointed out that the dissolution of the passive film is not frequently observed on the Ti3 surface but rather takes place randomly in certain locations. Table 4 lists the chemical compositions of feature positions marked in Fig. 10. A is a location on the flat surface of Ti7. Because



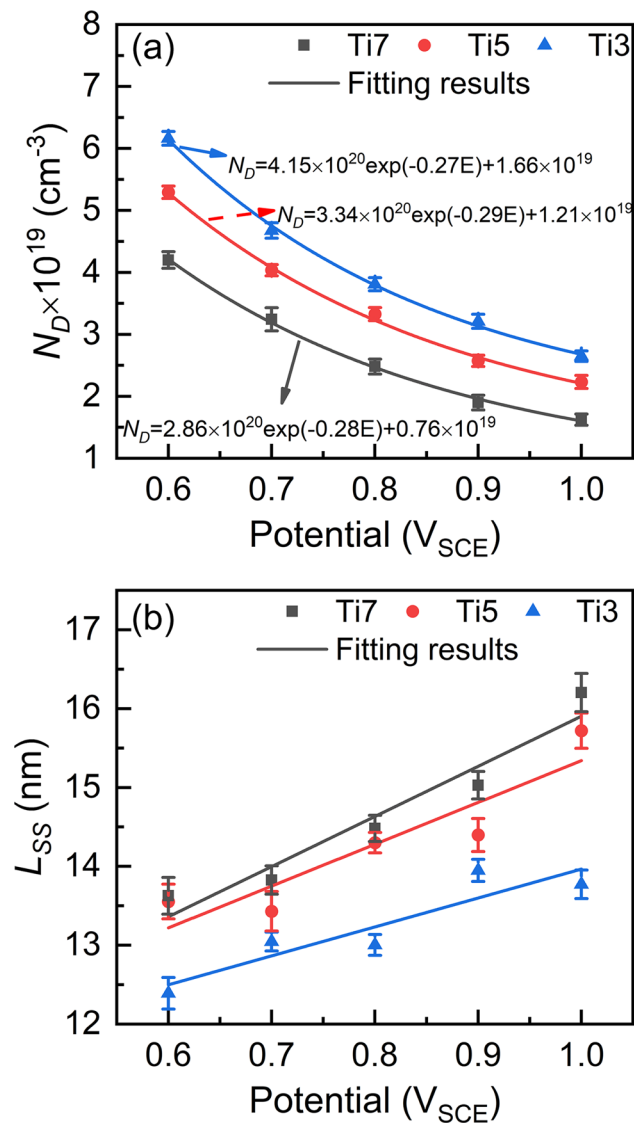


Fig. 8 Semiconductive properties of passive films on Ti7, Ti5 and Ti3 after potentiostatic polarization at 0.6–1 V: **a** donor densities, **b** thicknesses. Ti7, Ti5 and Ti3 indicate the samples in Hank's solutions with pH values of 7, 5, 3

of the formation of oxide film, O content reaches 8.2 at.%. B and C are the shallow pits on Ti5 and Ti3. The O contents of B and C points (7.3 at.%) are slightly lower than that of A point, possibly due to the pitting corrosion. D is a location of passive film dissolution. The O content further decreases to 6.1 at.%. On the one hand, since O is the primary component of the passive film, the dissolution of the film would lead to a decrease in O content within the examined area. On the other hand, the dissolution of the passive film also releases more ions.

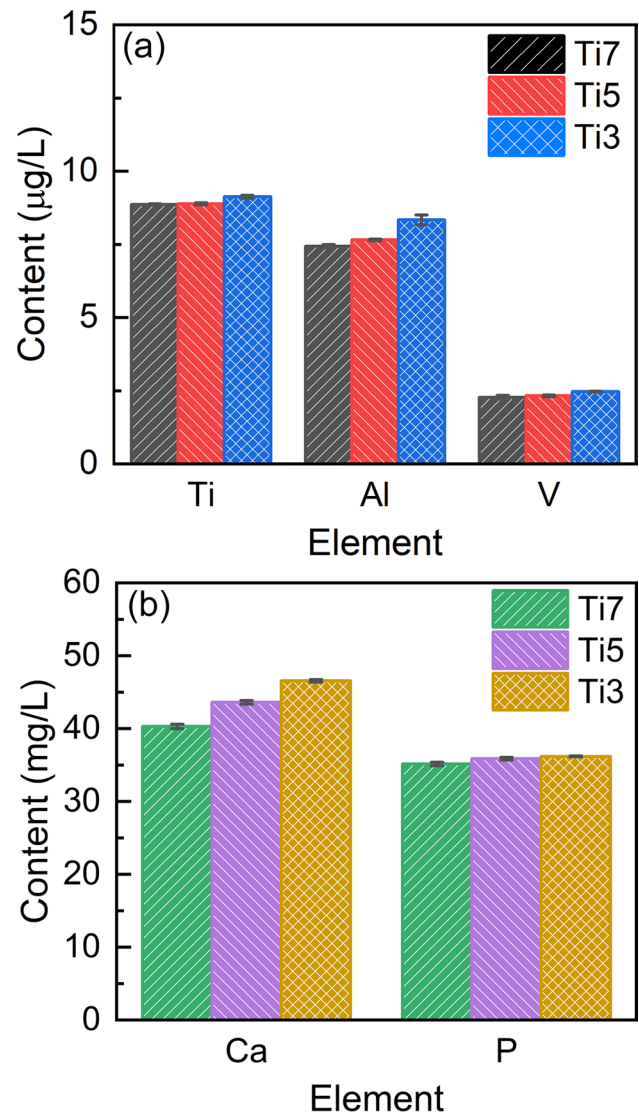


Fig. 9 Concentrations of Ti, Al, V, Ca and P ions from potentiostatic polarized samples under 0.6 V and 24 h immersion tests in Hank's solution: **a** Ti, Al and V, **b** Ca and P. Ti7, Ti5 and Ti3 indicate the samples in Hank's solutions with pH values of 7, 5 and 3

3.6 XPS Analysis

XPS was utilized to analyze and determine the compositions of the passive films on samples being potentiostatic polarized under 0.6 V after 1800 s. Figure 11 illustrates the fractions of Ti, Al, V, O, P, and Ca elements at different sputtering durations by XPS analysis. A substantial amount of O (i.e., 69.5 at.% for Ti7, 66.3 at.% for Ti5, 66.1 at.% for Ti3) has been detected on the surface of the specimens. This high proportion of O on the sample surface is ascribed to deposited calcium phosphate salt and passive film (mainly TiO_2) [52]. At durations of 10 s or less, the proportion of Ti significantly increases with the decrease in the proportion of O. However, beyond 10 s, P and Ca are barely detectable.

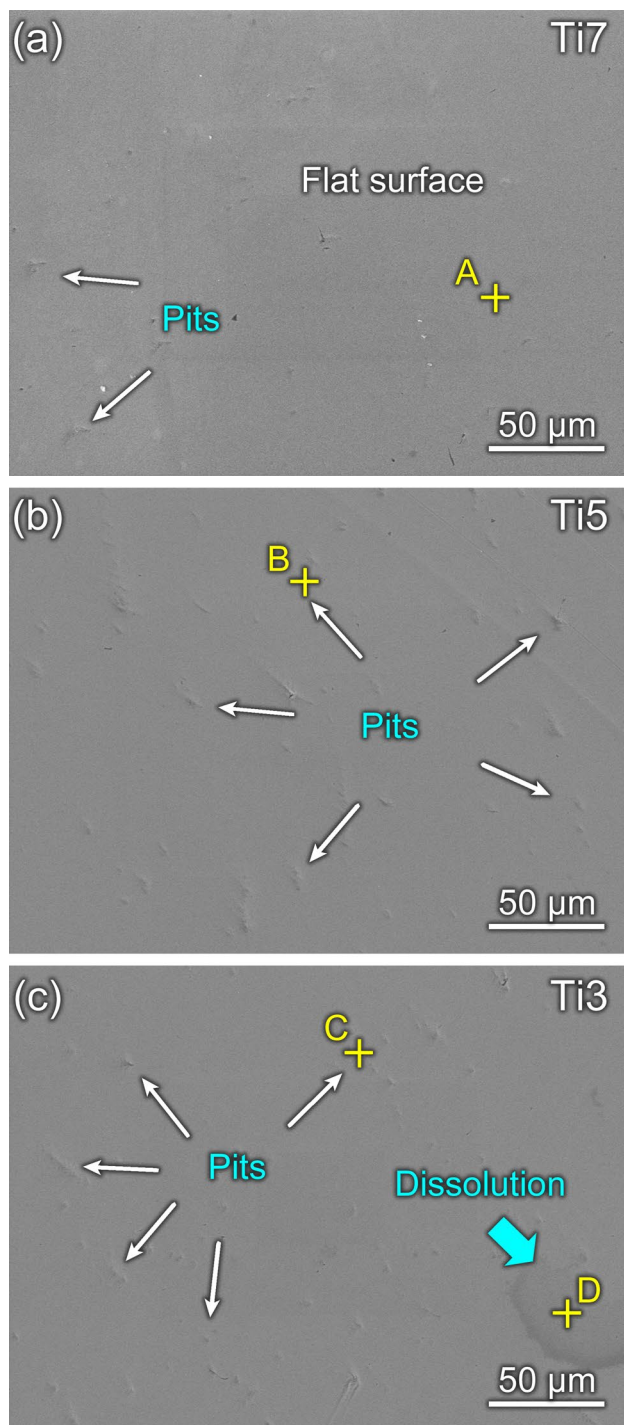


Fig. 10 Morphologies of potentiostatic polarized samples under 0.6 V and 24 h immersion tests: **a** Ti7, **b** Ti5, **c** Ti3. Ti7, Ti5 and Ti3 indicate the samples in Hank's solutions with pH values of 7, 5 and 3

With the increased sputtering time (and depth), the proportions of Ti and Al elevate while the O fraction decreases. This finding indicates the production of passive films on the sample surfaces obeys Fick's law [53, 54]. Moreover, V is scarcely detected within the passive films.

Table 4 Chemical compositions of feature positions marked in Fig. 10 (in at.%)

Feature position	Ti	Al	V	O
A	82.9	5.1	3.8	8.2
B	84.0	5.2	3.5	7.3
C	83.3	5.4	4	7.3
D	85.2	5.0	3.7	6.1

The passive films of samples predominantly comprise TiO_2 , Ti_2O_3 and TiO [48]. The Ti 2p spectra from various durations of the passive film were examined to explore the oxidation of the Ti matrix. Figure 12 portrays the deconvolution of the Ti 2p spectra collected at 0 s, 10 s, 30 s and 60 s, indicating that the binding energy of the characteristic peaks in the XPS spectrum shifts toward the lower side. This shift suggests a decrease in the Ti valence state, gradually changing from a fully-valent oxide to a non-filled valent oxide as sputtering time increases. The quantitative Ti oxide content in the passive film, obtained after deconvolution, is depicted in Fig. 13. Figure 12 demonstrates that the outermost Ti7, Ti5, and Ti3 layers exhibit the highest Ti^{4+} (TiO_2) content, which consistently decreases with depth. On the contrary, the fractions of Ti^{3+} (Ti_2O_3) and Ti^{2+} (TiO) augments with the sputtering depth. Gebert et al. [52] demonstrated that at the film/metal interface, Ti^{3+} and Ti^{2+} are continually formed and partially converted to the oxide TiO_2 in the highest valence state. Accordingly, the additional presence of Ti^{2+} (TiO) in Fig. 12b and c reveals that lactic acid addition to Hank's solution restricts the transformation of Ti^{2+} (TiO) to Ti^{4+} (TiO_2) and Ti^{3+} (Ti_2O_3). The oxide film sputtered for 10 s illustrates an increase in the Ti^{3+} (Ti_2O_3) fraction in the central regions of the passive films under all three conditions. With a rise in sputtering time, the Ti^{2+} (TiO) content grows, correlating with lactic acid concentration. At 60 s, Ti^0 is detected, suggesting that the sputtering depth surpasses the passive film thickness for all samples. The Ti^0 fractions attributed to Ti7, Ti5, and Ti3 after 60 s sputtering are 13.4 at.%, 21.3 at.%, and 27.8 at.%, respectively. These results demonstrate that a relatively thick passive film is generated on the Ti7 sample in Hank's solution without lactic acid addition, consistent with the L_{ss} result in Fig. 8b.

4 Discussion

4.1 Influence of Lactic Acid on the Corrosion Resistance of Samples

This work checks the corrosion behavior of TC4 specimens manufactured via L-PBF immersed in Hank's solutions with varying pH values regulated using lactic acid. Being a weak electrolyte, adding lactic acid results in ionization into

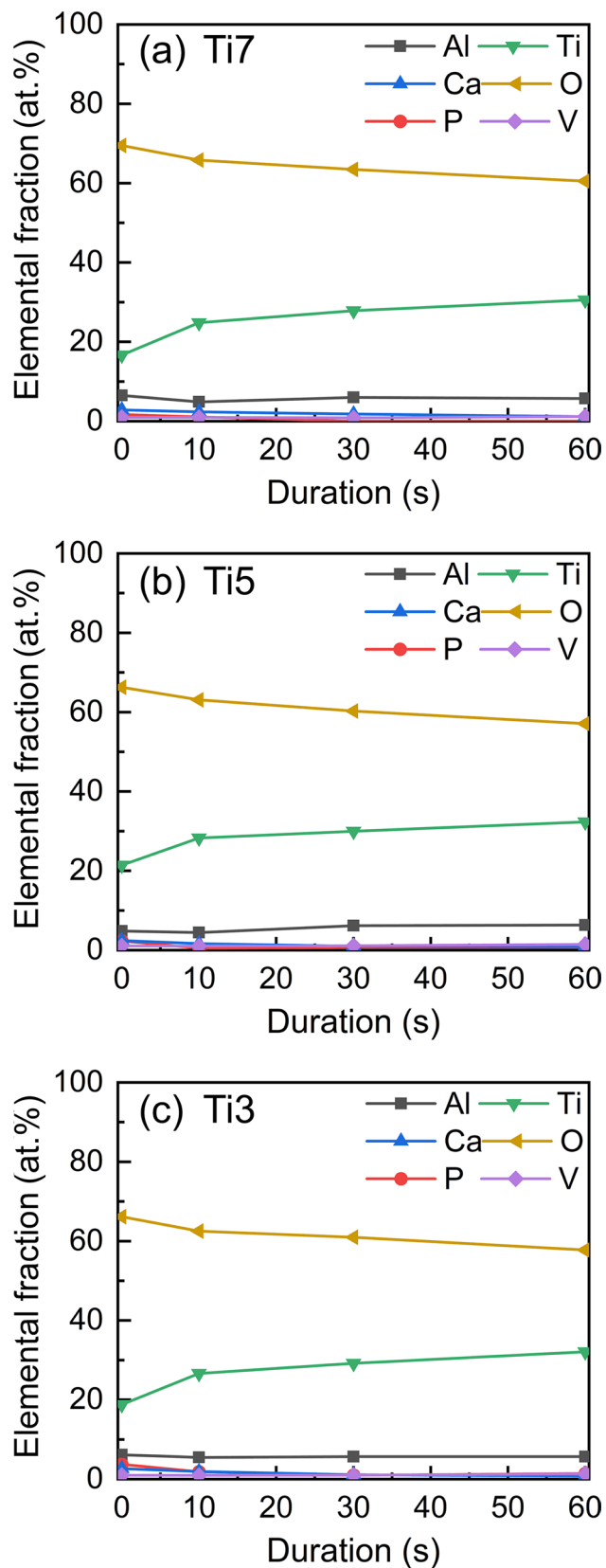


Fig. 11 Elemental fractions in the passive films at different durations: **a** Ti7, **b** Ti5, **c** Ti3 after potentiostatic polarization under 0.6 V. Ti7, Ti5 and Ti3 indicate the samples in Hank's solutions with pH values of 7, 5 and 3

lactate ions ($\text{CH}_3\text{CH}(\text{OH})\text{COO}^-$) and H^+ in the solution. The abbreviation L^- denotes $\text{CH}_3\text{CH}(\text{OH})\text{COO}^-$. Evaluation of the general corrosion behavior of passive metals entails an examination of the corrosion rate and the protection mechanism of the resulting passive film. As such, the investigation of the impact of lactic acid on the corrosion behavior of the TC4 specimens involved in this research will primarily be focused on these two aspects.

The OCP values of the samples obtained demonstrated an increase in association with the lactic acid contents, as depicted in Fig. 2. Such a phenomenon is attributed to the surface adsorption of lactic acid, which causes a shift in OCP toward a positive value. Furthermore, the OCP values indicate the trends in the film formation of the samples during the first 1800 s of immersion, illustrating that adding lactic acid inhibits the formation of the passive films. Owing to the high chemical activity of Ti alloys, the passive films are formed on the samples, resulting in a gradual increase in their OCP curves [55]. Qu et al. [23] reported similar results, observing that the OCP values of commercially pure Ti are shifted toward a more positive value after adding lactic acid in simulated artificial saliva. They also discovered that the OCP values of the samples declined after one-day immersion, indicating the sluggish dissolution of passive films present in the (lactic acid)-containing solution.

All samples have a typical activation-passivation phenomenon exhibited in the potentiodynamic polarization. The corrosion potentials of the samples are observed in the following sequence: $\text{Ti3} > \text{Ti5} > \text{Ti7}$, which is consistent with their OCP value outcomes, as displayed in Fig. 4. The corrosion potentials of samples are lower than 0 V, indicating that the corrosion would take place spontaneously in the corrosion environments used [56]. Consequently, the corrosion densities of the samples would determine their corresponding corrosion rates. The calculated results in Table 2 reveal that Ti3 has the highest corrosion rate while Ti7 has the lowest. Hence, it is substantially demonstrated that lactic acid accelerates the corrosion of L-PBF-produced TC4. The EIS tests conducted following the OCP tests illustrate that the corrosion resistance of the samples can be determined by evaluating the values of R_{ct} . According to the equivalent electrical circuit model in Fig. 3, the charge transfer resistance R_{ct} specifies the difficulty in electron transfer from the sample to the solution [14]. The sample Ti3 exhibits the lowest R_{ct} value among the samples, indicating that the formed passive films provide inadequate protection and result in the highest corrosion rate for the sample. As depicted in Figs. 5 and 6, a comparable situation is also found for the passive films on samples produced by potentiostatic polarization. At different applied potentials, the i_{ss} of Ti3 exceeds those of Ti5 and Ti7. Typically, the i_{ss} indicates the ratio between the applied potential and the impedance of the oxide film. Therefore, it can be inferred that the (lactic acid)-containing

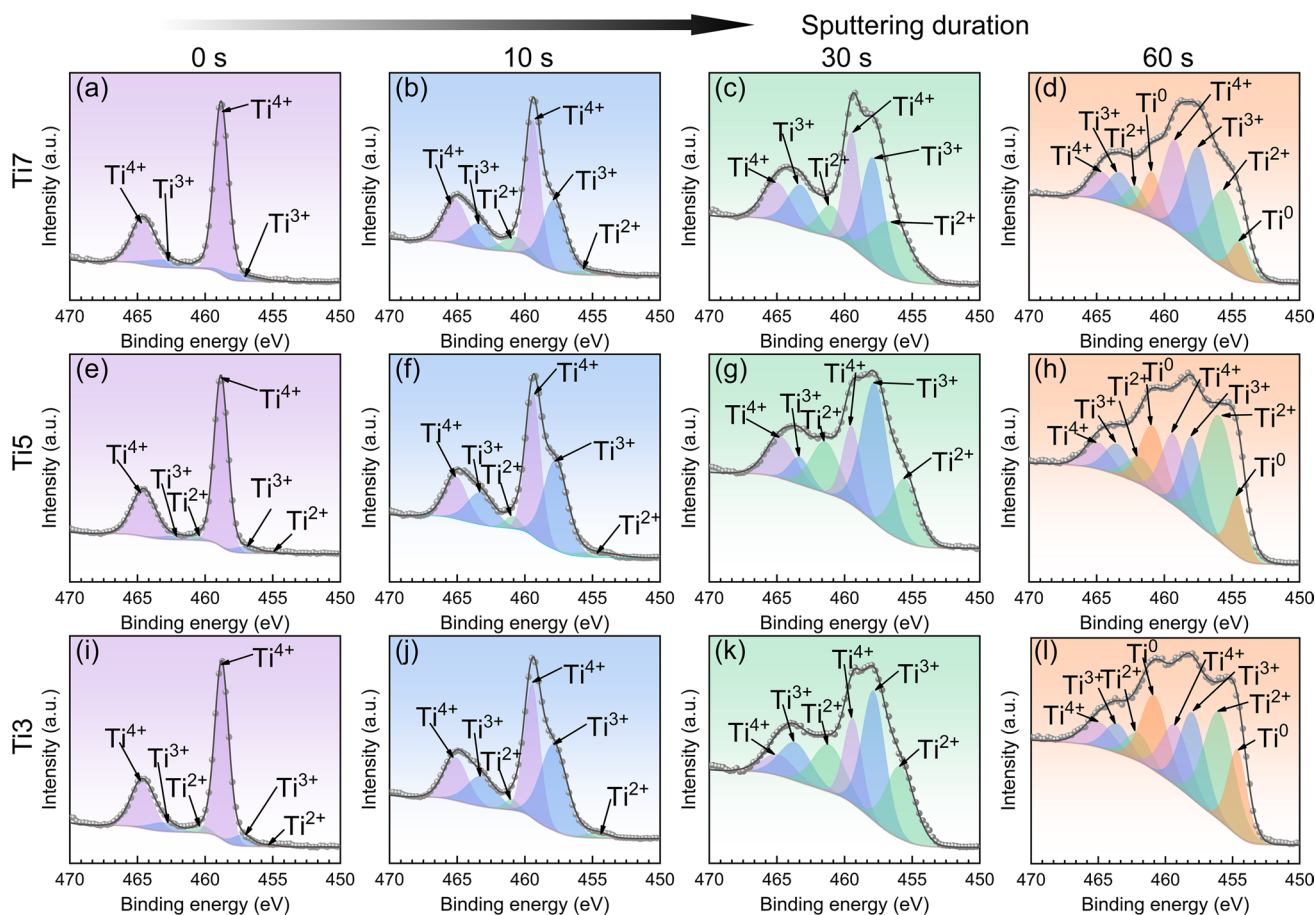


Fig. 12 Deconvoluted XPS spectra of Ti 2p region for the samples after potentiostatic polarization under 0.6 V in Hank's solution with the pH value of 7, 5 and 3, respectively. Ti7, Ti5 and Ti3 indicate the samples in Hank's solutions with pH values of 7, 5 and 3

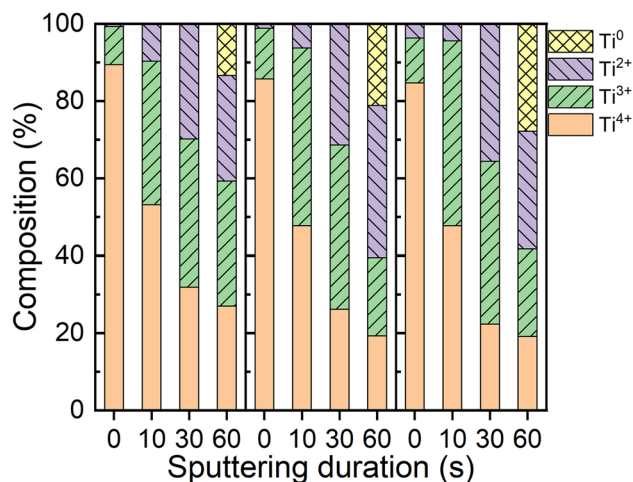


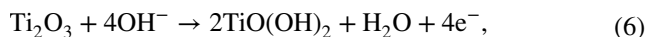
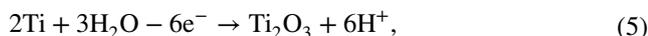
Fig. 13 Proportions of titanium ions with varying valence in the passive films on the samples after potentiostatic polarization under 0.6 V in Hank's solution with the pH value of 7, 5 and 3 at different sputtering durations. Ti7, Ti5 and Ti3 indicate the samples in Hank's solutions with pH values of 7, 5 and 3

Hank's solution would cause a degradation of the passive film on Ti alloys. Benea et al. [21] reported that adsorbed lactic acid could impede passive film production. Hence, the thicknesses of passive films formed on the samples immersed in the (lactic acid)-containing Hank's solution and their impedance are comparatively lower (Fig. 8b and Table 3). Additionally, the sample corrosion resistance decreases with increased lactic acid content, which becomes more pronounced with higher lactic acid concentrations, as depicted in Fig. 5.

4.2 Production and Dissolution of Passive Film Induced by Lactic Acid

The production of a passive film takes place owing to the movements of metal ions and oxygen vacancies between the metal/film interface and film/solution interface [37]. From the XPS analysis provided in Figs. 12 and 13, it becomes evident that TiO_2 (Ti^{4+}), Ti_2O_3 (Ti^{3+}), and TiO (Ti^{2+}) in the passive films alternatively become the primary components from the outer layer to the inner layer, illustrating a gradual

oxidation process [37]. The process of forming the oxide film can be described in three stages [45]: (a) at the onset of corrosion, TiO is produced on the Ti alloy surface, then oxidizing to a trivalent state (Ti_2O_3), as presented in Eq. (5); (b) the formed trivalent state (Ti_2O_3) further transforms into a tetravalent state ($\text{TiO}(\text{OH})_2$) before dehydration, as illustrated in Eq. (6); (c) ultimately, $\text{TiO}(\text{OH})_2$ undergoes dehydration, subsequently forming the most stable oxide (TiO_2), as demonstrated in Eq. (7):

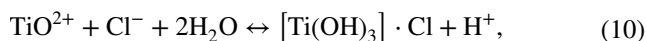


Further observations from Figs. 12 and 13 indicate that Ti3 exhibits a diminished proportion of Ti^{4+} in the outermost layer of the passive film. Two aspects should be considered to comprehend this phenomenon. The first aspect is the conversion of Ti^{4+} from Ti^{3+} and Ti^{2+} in the passive film [45]. The second aspect is the dissolution of TiO_2 on the film surface [14]. Generally, these two reasons proceed concomitantly.

The oxygen vacancies exhibit considerably faster movement than metal vacancies, resulting in a surface accumulation of numerous metal vacancies on the passive film surface [50]. As such, the surface of the passive film formed on the metal usually exhibits a negative charge [50]. Consequently, H^+ in the solution tends to be trapped, promoting the dissolution of the passive film caused by the reaction expressed in Eq. (8). Furthermore, with an increase in the lactic acid content (resulting in decreased pH values and increased H^+ concentrations), the dissolution of the passive film becomes pronounced [57]:



Adding lactic acid leads to an alternative method of passive film dissolution. Due to the dissolution balance (Eq. (9)), TiO_2 has weak solubility in the aqueous solution [58]. However, TiO^{2+} is unstable in solutions containing Cl^- and would be easily hydrolyzed, as shown in Eq. (10).



In the (lactic acid)-containing solutions, the ionized lactate ion (L^-) causes the following reactions (Eq. (11)) [23]:



It has been observed that L^- readily forms a chelate compound with Ti and dissolves into the solution, thereby accelerating the dissolution of TiO_2 on the surface of the passive film [23]. Such findings suggest that the amount of released Ti^{4+} ions would increase in lactic acid solutions. As stated in Sect. 4.1, the adsorbed lactic acid can potentially hinder the formation of the passive film, thereby impeding the conversion of Ti^{4+} from Ti^{3+} and Ti^{2+} in the passive film. Electroneutrality principles priori suggest that Ti^{3+} and Ti^{2+} can initiate or stabilize oxygen vacancies at specific sites [49]. Therefore, the passive films on Ti3 and Ti5 exhibit a higher fraction of Ti^{3+} and Ti^{2+} (Figs. 12 and 13), showing higher donor densities than Ti7 (Fig. 8a).

Notably, compared to Ti^{4+} , Ti^{3+} and Ti^{2+} exhibit higher affinity with O^{2-} and are less susceptible to being expelled from the passive film in aqueous solutions. Consequently, fewer titanium ions were detected in Hank's solution following a 24 h immersion of potentiostatically polarized samples, as indicated in Fig. 9a. Oxygen vacancies within the film could trap anions in Hank's solution [48]. Unlike Cl^- , L^- is too bulky to occupy the oxygen vacancy. Therefore, L^- can bind to the film surface and impede the ion transportation between the film and solution, resulting in the slower formation and dissolution of passive films. Enhanced OCP values of samples and released ions in the solution (Figs. 2 and 9a) are primary evidence of this phenomenon.

As a weak electrolyte, ionized H^+ significantly influences the passive film and deposited salts. When immersed in simulated body fluids or Hank's solution, calcium phosphates are often deposited on the sample surface [46]. The presence of H^+ can react with calcium phosphates and create soluble salts, resulting in increased Ca and P detected in immersion test solutions (Fig. 9b). Higher levels of lactic acid content foster an increased quantity of Ca and P found in the solution. Notably, the deposition of calcium phosphates strongly affects osseointegration [51], while hindering their deposition could delay patient rehabilitation post-implantation. Furthermore, H^+ reacts according to Eq. (8), destroying the passive films upon contact. Compared to other strong acids, lactic acid only locally destroys the passive films on Ti alloys [20, 21, 23]. Mabileau et al. [20] found that immersing Ti in artificial saliva containing lactic acid for 21 days would significantly increase Ti surface roughness due to local passive film destruction by H^+ . Benea et al. [21] similarly observed identical results following a 168-h immersion of TC4 in Hank's solution containing lactic acid. In this work, regardless of the film formation potential, the impedance of the passive film decreases as the lactic acid content increases. Hence, one may conclude that although adding lactic acid increases OCP and corrosion potential while simultaneously reducing ion release, long-term immersion gradually degrades the formed passive film.

5 Conclusions

The corrosion behavior of Ti-6Al-4V (TC4) samples fabricated using laser powder bed fusion (L-PBF) in Hank's solution with (pH = 3, pH = 5) and without (pH = 7) lactic acid at 37 °C was investigated. Meanwhile, the production and dissolution of passive films and the ion release were also investigated. The following outcomes can be derived:

1. The addition of lactic acid is shown to decrease the corrosion resistance of samples by deteriorating the passive film that has formed. The corrosion current density of the samples rises from $0.12 \pm 0.02 \mu\text{A cm}^{-2}$ to $0.18 \pm 0.03 \mu\text{A cm}^{-2}$ as the pH value drops from 7 to 3. Correspondingly, the impedance of the formed passive film after the open circuit potential test decreases from $1.07 \pm 0.24 \text{ M}\Omega \text{ cm}^2$ to $0.22 \pm 0.14 \text{ M}\Omega \text{ cm}^2$ as the lactic acid content increases.
2. The impedance of the passive film formed by potentiostatic polarization also decreases with increased lactic acid content. The highest density of oxygen vacancies, which act as donors, was observed in the passive film, and the lowest thickness was under Hank's solution, with a pH value of 3. Consequently, the sample immersed in Hank's solution at a pH value of 3 showed the highest quasi-steady-state current density compared to counterparts receiving similar treatment.
3. As a weak electrolyte, lactic acid undergoes ionization in the solution to produce lactate ions and H^+ . It is postulated that adsorbed lactate ions would increase the open circuit potential and alleviate ion release in the short term. On the other hand, the presence of H^+ impedes the deposition of calcium phosphates on the surfaces of immersed samples over 24 h. Consequently, the existence of lactic acid may detrimentally affect patient recovery following implantation.
4. XPS examination showed a reduced percentage of Ti^{4+} but increased Ti^{3+} and Ti^{2+} on the sample surface immersed in Hank's solution with a pH value of 3 after potentiostatic polarization. These findings, in conjunction with ion release results, suggest that lactic acid may hinder the conversion of Ti^{4+} to Ti^{3+} and Ti^{2+} .

Acknowledgements The authors acknowledge the Fundamental Research Program of Jiangsu Province (BK20201000), the Australian Research Council through the Discovery Project (DP110101653, DP130103592), the Basic and Applied Basic Research Foundation of Guangdong Province, China (2022A1515140123, 2021A1515110729) and the Foshan (Southern China) Institute for New Materials (2021AYF25017). The authors are grateful to Jinling Zhu.

Data availability The raw/processed data required to reproduce these findings cannot be shared at this time as the data also forms part of an ongoing study.

Declarations

Conflict of interest The authors state that there are no conflict of interest to disclose.

References

- [1] P. Qin, L.Y. Chen, C.H. Zhao, Y.J. Liu, C.D. Cao, H. Sun, L.C. Zhang, *Corros. Sci.* **189**, 109609 (2021)
- [2] S. Qin, X. Xu, Y. Lu, L. Li, T. Huang, J. Lin, *Acta Metall. Sin.-Engl. Lett.* **35**, 812 (2022)
- [3] L.C. Zhang, L.Y. Chen, *Adv. Eng. Mater.* **21**, 801215 (2019)
- [4] S.B. Sun, L.J. Zheng, J.H. Liu, H. Zhang, *Rare Met.* **42**, 1353 (2023)
- [5] P. Qin, Y. Liu, T.B. Sercombe, Y. Li, C. Zhang, C. Cao, H. Sun, L.C. Zhang, *A.C.S. Biomater. Sci. Eng.* **4**, 2633 (2018)
- [6] C. Xu, L.Y. Chen, C. Zheng, Z.Y. Zhang, R. Li, H.Y. Yang, J. Peng, L. Zhang, L.C. Zhang, *Adv. Eng. Mater.* **24**, 2200674 (2022)
- [7] L.Y. Chen, S.X. Liang, Y. Liu, L.C. Zhang, *Mater. Sci. Eng. R Rep.* **146**, 100648 (2021)
- [8] X.N. Hao, X. Liu, *Rare Met.* **41**, 3677 (2022)
- [9] C. Xu, Y. Peng, L.Y. Chen, T.Y. Zhang, S. He, K.H. Wang, *Corros. Sci.* **215**, 111048 (2023)
- [10] X. Jin, P. Ye, H. Ji, Z. Suo, B. Wei, X. Li, W. Fang, *Int. J. Miner. Metall. Mater.* **29**, 2232 (2022)
- [11] D.C. Rodrigues, P. Valderrama, T.G. Wilson, K. Palmer, A. Thomas, S. Sridhar, A. Adapalli, M. Burbano, C. Wadhvani, *Materials* **6**, 5258 (2013)
- [12] Z. Guo, X. Shen, F. Liu, J. Guan, Y. Zhang, F. Dong, Y. Wang, X. Yuan, B. Wang, L. Luo, Y. Su, J. Cheng, *J. Alloys Compd.* **960**, 170739 (2023)
- [13] J.C.M. Souza, K. Apaza-Bedoya, C.A.M. Benfatti, F.S. Silva, B. Henriques, *Metals* **10**, 1272 (2020)
- [14] L.Y. Chen, H.Y. Zhang, C. Zheng, H.Y. Yang, P. Qin, C. Zhao, S. Lu, S.X. Liang, L. Chai, L.C. Zhang, *Mater. Des.* **208**, 109907 (2021)
- [15] Y.W. Cui, L.Y. Chen, P. Qin, R. Li, Q. Zang, J. Peng, L. Zhang, S. Lu, L. Wang, L.C. Zhang, *Corros. Sci.* **203**, 110333 (2022)
- [16] M. Cabrini, A. Carrozza, S. Lorenzi, T. Pastore, C. Testa, D. Manfredi, P. Fino, F. Scenini, *J. Mater. Process. Technol.* **308**, 117730 (2022)
- [17] P.A. Mashimo, Y. Yamamoto, M. Nakamura, H.S. Reynolds, R.J. Genco, *J. Periodont.* **56**, 548 (1985)
- [18] P.D. Marsh, *Adv. Dent. Res.* **8**, 263 (1994)
- [19] M.A. Houle, D. Grenier, *Med. Mal. Infect.* **33**, 331 (2003)
- [20] G. Mabilieu, S. Bourdon, M.L. Joly-Guillou, R. Filmon, M.F. Baslé, D. Chappard, *Acta Biomater.* **2**, 121 (2006)
- [21] L. Benea, N. Simionescu-Bogatu, *Materials* **14**, 7404 (2021)
- [22] A. Banu, L. Preda, M. Marcu, L.L. Dinca, M.E. Maxim, G. Dobri, *Metal. Mater. Trans. A* **53**, 2060 (2022)
- [23] Q. Qu, L. Wang, Y. Chen, L. Li, Y. He, Z. Ding, *Materials* **7**, 5528 (2014)
- [24] H. Mirzadeh, *Int. J. Miner. Metall. Mater.* **30**, 1278 (2023)
- [25] S. Liu, Y.C. Shin, *Mater. Des.* **164**, 107552 (2019)
- [26] W. Xu, M. Brandt, S. Sun, J. Elambasseril, Q. Liu, K. Latham, K. Xia, M. Qian, *Acta Mater.* **85**, 74 (2015)
- [27] H.Y. Yang, Z. Wang, L.Y. Chen, S.L. Shu, F. Qiu, L.C. Zhang, *Compos. Part B: Eng.* **209**, 108605 (2021)
- [28] L.C. Zhang, H. Attar, *Adv. Eng. Mater.* **18**, 463 (2016)
- [29] L. Chen, J. Li, Y. Zhang, W. Lu, L.C. Zhang, L. Wang, D. Zhang, *J. Nucl. Sci. Technol.* **53**, 496 (2016)
- [30] Y. Bai, X. Gai, S. Li, L.C. Zhang, Y. Liu, Y. Hao, X. Zhang, R. Yang, Y. Gao, *Corros. Sci.* **123**, 289 (2017)

- [31] N. Dai, L.C. Zhang, J. Zhang, Q. Chen, M. Wu, *Corros. Sci.* **102**, 484 (2016)
- [32] C. Man, C. Dong, T. Liu, D. Kong, D. Wang, X. Li, *Appl. Surf. Sci.* **467**, 193 (2019)
- [33] C. Man, C. Dong, Z. Cui, K. Xiao, Q. Yu, X. Li, *Appl. Surf. Sci.* **427**, 763 (2018)
- [34] P. Sang, L.Y. Chen, C. Zhao, Z.-X. Wang, H. Wang, S. Lu, D. Song, J.H. Xu, L.C. Zhang, *Metals* **9**, 1342 (2019)
- [35] Y. Xu, M.Y. Tan, *Corros. Sci.* **151**, 163 (2019)
- [36] D.S. Kong, J.X. Wu, *J. Electro. Soc.* **155**, C32 (2008)
- [37] X. Gai, Y. Bai, J. Li, S. Li, W. Hou, Y. Hao, X. Zhang, R. Yang, R.D.K. Misra, *Corros. Sci.* **145**, 80 (2018)
- [38] M. Lakatos-Varsányi, F. Falkenberg, I. Olefjord, *Electrochim. Acta* **43**, 187 (1998)
- [39] N. Dai, L.C. Zhang, J. Zhang, X. Zhang, Q. Ni, Y. Chen, M. Wu, C. Yang, *Corros. Sci.* **111**, 703 (2016)
- [40] R. Chelariu, G. Bolat, J. Izquierdo, D. Mareci, D.M. Gordin, T. Gloriant, R.M. Souto, *Electrochim. Acta* **137**, 280 (2014)
- [41] G. Bolat, D. Mareci, R. Chelariu, J. Izquierdo, S. González, R.M. Souto, *Electrochim. Acta* **113**, 470 (2013)
- [42] D.D. Macdonald, *Electrochim. Acta* **56**, 1761 (2011)
- [43] R.M. Fernández-Domene, E. Blasco-Tamarit, D.M. García-García, J. García-Antón, *Electrochim. Acta* **95**, 1 (2013)
- [44] Z. Duan, C. Man, C. Dong, Z. Cui, D. Kong, L. Wang, X. Wang, *Corros. Sci.* **167**, 108520 (2020)
- [45] P. Qin, L.Y. Chen, Y.J. Liu, Z. Jia, S.X. Liang, C.H. Zhao, H. Sun, L.C. Zhang, *Corros. Sci.* **191**, 109728 (2021)
- [46] T. Hanawa, *Mater. Sci. Eng. C* **24**, 745 (2004)
- [47] R. Azadbakht, T. Almasi, H. Keypour, M. Rezaeivala, *Inorg. Chem. Com.* **33**, 63 (2013)
- [48] Y.W. Cui, L.Y. Chen, Y.H. Chu, L. Zhang, R. Li, S. Lu, L. Wang, L.C. Zhang, *Corros. Sci.* **215**, 111017 (2023)
- [49] L. Chen, J. Li, Y. Zhang, L.C. Zhang, W. Lu, L. Zhang, L. Wang, D. Zhang, *Corros. Sci.* **100**, 651 (2015)
- [50] L. Guan, Y. Li, G. Wang, Y. Zhang, L.C. Zhang, *Electrochim. Acta* **285**, 172 (2018)
- [51] L.C. Zhang, L.Y. Chen, L. Wang, *Adv. Eng. Mater.* **22**, 1901258 (2020)
- [52] T. Hanawa, M. Ota, *Appl. Surf. Sci.* **55**, 269 (1992)
- [53] L. Zhang, L.Y. Chen, C. Zhao, Y. Liu, L.C. Zhang, *Metals* **9**, 850 (2019)
- [54] Z. Jiang, X. Dai, T. Norby, H. Middleton, *Corros. Sci.* **53**, 815 (2011)
- [55] Z.R. Ye, Z.C. Qiu, Z.B. Wang, Y.G. Zheng, R. Yi, X. Zhou, *Acta Metall. Sin. (Engl. Lett.)* **33**, 839 (2020)
- [56] C. Liu, Y. Li, X. Cheng, X. Li, *Acta Metall. Sin. (Engl. Lett.)* **35**, 1055 (2022)
- [57] Y. Cui, L. Chen, L. Wang, J. Cheng, L. Zhang, *Metals* **13**, 415 (2023)
- [58] O.E.M. Pohler, *Injury* **31**, D7 (2000)

Springer Nature or its licensor (e.g. a society or other partner) holds exclusive rights to this article under a publishing agreement with the author(s) or other rightsholder(s); author self-archiving of the accepted manuscript version of this article is solely governed by the terms of such publishing agreement and applicable law.